




Susceptibility synthesis of arbitrary shaped metasurfaces

N. Lebbe ^{1,*}, S. Lanteri ¹, S. Y. Golla,² and P. Genevet ²

¹Université Côte d'Azur, Inria, CNRS, LJAD, 06902 Sophia Antipolis Cedex, France

²Université Côte d'Azur, CNRS, CRHEA, Rue Bernard Gregory, Sophia Antipolis, 06560 Valbonne, France



(Received 27 August 2021; revised 4 April 2022; accepted 21 June 2022; published 7 July 2022)

Visual perception relies on light scattering at the object's surface in the direction of observation. By engineering the surface scattering properties, it is possible to realize arbitrary visual percepts. Here, we address theoretically this problem of electromagnetic field transition conditions at conformal interfaces to achieve surface-topography-dependent transmitted and reflected fields. Our analysis, supported by two- and three-dimensional finite-element simulations, provides a solid theoretical framework to design metasurfaces for cloaking, wearable optics, and next-generation freeform imaging systems.

DOI: [10.1103/PhysRevB.106.035110](https://doi.org/10.1103/PhysRevB.106.035110)

I. INTRODUCTION

For centuries, optical design consisted of developing thin films and various coatings to address light reflection, transmission, and/or diffusion at interfaces. Developments in nanophotonics have strongly improved our ability to control light scattering processes with optically resonant nanostructures. Artificial optical materials, also dubbed metamaterials and metasurfaces, presenting unexpected light propagation effects have been realized, leading to cloaking [1], negative refraction [2,3], subwavelength focusing, generalized refraction [4], and vectorial electromagnetic field control [5–8]. Today these “conventional” metamaterials and metasurfaces are realized assembling subwavelength photonic structures. The study of the device's optical response is generally complex and requires lengthy numerical simulations that describe in detail the effect of light interaction with a large number of nanophotonic building blocks. To avoid modeling thousands and billions of small geometric features, homogenization methods that approximate the complexity of an inhomogeneous material filled with nanoscale inclusions by its effective medium response, i.e., homogeneous artificial material, have been proposed [9,10]. For the case of metasurfaces, consisting of a surface two-dimensional arrangement of nanostructures, equivalent transition conditions linking the values of the macroscopic field quantities on both sides of a thin homogenized layer have been derived. In fact, such transition conditions are well known in electromagnetics but also in acoustics and are commonly used to simplify physical interpretation or ease numerical simulations [11–13]. Metasurfaces have thus been modeled using advanced effective transition conditions, called generalized sheet transition conditions (GSTCs). GSTCs were originally derived in optics in the 1990s in the seminal paper of Idemen [14]. These transition conditions conceal in a tensorial form the equivalent

response occurring on reflecting and transmitting fields at complex interfaces. Efforts to reproduce the above-mentioned intriguing effects using GSTC formulation, including anomalous refraction, cloaking, and vectorial electromagnetic field control, have been realized recently [15,16]. But so far, modeling relied on Idemen's original work, and most papers dealing with GSTCs only considered layers manufactured on planar surfaces.

Here, we provide a fully self-contained introduction to GSTCs on arbitrary geometries—namely, conformal GSTCs (C-GSTCs)—with all the necessary theoretical and numerical tools to exploit these transition conditions. A schematic of the studied problem is presented in Fig. 1. Inspired by Idemen's original idea to calculate the reflection and transmission properties of field discontinuity at planar interfaces, our derivation considers both electric and magnetic surface distributions on a shaped surface (see formal description in [17]). We express these quantities in the sense of the distribution function along the surface. After deriving the C-GSTCs, we explain the inversion procedure to synthesize the susceptibilities of conformal interfaces for arbitrary input-output fields. Finally, a numerical implementation of these expressions using a finite-element method (FEM) is realized to study the angular sensitivity of simple metasurfaces, including deflector and lenses, and we also propose a generic method for surface cloaking of complex objects.

Compared to the existing literature on GSTCs, this article contributes to the domain in three ways:

(1) We generalize the susceptibility synthesis method to the conformal case by considering susceptibility tensors distributed on surfaces of arbitrary shapes. To obtain the GSTC in curvilinear coordinates, an extension of the classical method based on surface distribution is described.

(2) We provide a full two- and three-dimensional implementation of GSTC on arbitrary interfaces using the FEM through the use of the variational formulation associated with Maxwell equations and GSTC.

(3) We present numerical examples showing the versatility of the synthesis method in multiple scenarios.

*Corresponding author: lebbe.nicolas@gmail.com

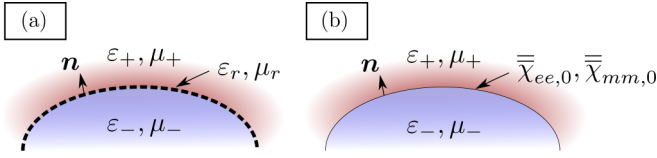


FIG. 1. Schematic representation of conformal metasurfaces. (a) Light reflection and refraction across a conformal metasurface defined by an ensemble of nanostructured materials along the curved surface. (b) The conformal metasurface is modeled using equivalent GSTCs and the associated physical properties defined along the surface to satisfy the input-output field discontinuities.

II. DERIVATION OF CONFORMAL GSTCs USING SURFACE DISTRIBUTIONS

We consider Maxwell's equations in the time-harmonic regime assuming a time dependency in $\exp(+j\omega t)$:

$$\begin{aligned} \nabla \times \mathbf{E} &= -j\omega \mathbf{B}, & \nabla \times \mathbf{H} &= j\omega \mathbf{D}, \\ \nabla \cdot \mathbf{D} &= 0, & \nabla \cdot \mathbf{B} &= 0, \end{aligned} \quad (1)$$

together with the following (simply anisotropic) constitutive relations linking the electromagnetic fields with the electric and magnetic inductions through electric and magnetic susceptibility tensors:

$$\mathbf{D} = \epsilon_0(\bar{\chi}_{ee} + 1)\mathbf{E} \quad \text{and} \quad \mathbf{B} = \mu_0(\bar{\chi}_{mm} + 1)\mathbf{H}. \quad (2)$$

With these definitions, the electromagnetic fields satisfy the following natural transition conditions at the interface between two media:

$$\mathbf{n} \times \llbracket \mathbf{E} \rrbracket = \mathbf{0}, \quad \mathbf{n} \times \llbracket \mathbf{H} \rrbracket = \mathbf{0}, \quad \mathbf{n} \cdot \llbracket \mathbf{D} \rrbracket = 0, \quad \mathbf{n} \cdot \llbracket \mathbf{B} \rrbracket = 0,$$

where for any field $\mathbf{A} = \mathbf{E}, \mathbf{H}, \mathbf{D}, \mathbf{B}$, the jump operator $\llbracket \mathbf{A} \rrbracket = \mathbf{A}_+ - \mathbf{A}_-$ with \mathbf{A}_\pm the values of \mathbf{A} above and below the interface. With a metasurface, however, the interface is covered with resonant nanostructures of various geometries that can resonantly interact with the incident light, inducing localized surface electric and magnetic dipole moments at the interface plane responsible for electromagnetic field discontinuities. This interaction modifies the natural transition conditions. The derivation of C-GSTCs begins by considering that discontinuities may be formally treated by decomposing the fields according to a series of n th derivatives of Dirac delta functions $\delta_S^{(n)}$ defined along the surface (a proper mathematical definition of this distribution is provided in Sec. II of the Supplemental Material [17]). We consider here an arbitrary conformal metasurface located on a two-dimensional surface $S = \{\mathbf{x} = (x, y, z), z = f(x, y)\}$, as presented in Fig. 1, and assume that each field \mathbf{A} can be decomposed as a series of Dirac surface distributions δ_S with multiple singular parts and one regular part as follows:

$$\mathbf{A}(\mathbf{x}) = \bar{\mathbf{A}}(\mathbf{x}) + \sum_{n=0}^{\infty} \mathbf{A}_n(x, y) \delta_S^{(n)}(\mathbf{x}), \quad (3)$$

where the \mathbf{A}_n are the singular parts of \mathbf{A} defined on the conformal interface while the regular part $\bar{\mathbf{A}}$ is given by

$$\bar{\mathbf{A}}(\mathbf{x}) = \mathbf{A}_+(\mathbf{x}) \text{ if } z > f(x, y) \text{ and } \mathbf{A}_-(\mathbf{x}) \text{ if } z < f(x, y).$$

Now and for the remainder of this paper, we will consider that $\mathbf{A}_n = \mathbf{0}$ for $n > 0$ (this is due to the fact that we are only interested in the first-order transition conditions verified by the fields). By substituting the distribution form of the fields from (3) into Maxwell equations (1) and using the identities discussed in Sec. II of the Supplemental Material [17], which provide the curl and divergence of singular fields, we then find that

$$\begin{aligned} (\nabla_{\parallel} \times \mathbf{E}_0) \delta_S + \mathbf{n} \times \mathbf{E}_0 \partial_n \delta_S + \overline{\nabla \times \mathbf{E}} + \mathbf{n} \times \llbracket \mathbf{E} \rrbracket \delta_S \\ = -j\omega(\mathbf{B}_0 \delta_S + \bar{\mathbf{B}}), \end{aligned} \quad (4)$$

$$\begin{aligned} (\nabla_{\parallel} \times \mathbf{H}_0) \delta_S + \mathbf{n} \times \mathbf{H}_0 \partial_n \delta_S + \overline{\nabla \times \mathbf{H}} + \mathbf{n} \times \llbracket \mathbf{H} \rrbracket \delta_S \\ = j\omega(\mathbf{D}_0 \delta_S + \bar{\mathbf{D}}), \end{aligned} \quad (5)$$

$$(\nabla_{\parallel} \cdot \mathbf{D}_0) \delta_S + \mathbf{n} \cdot \mathbf{D}_0 \partial_n \delta_S + \overline{\nabla \cdot \mathbf{D}} + \mathbf{n} \cdot \llbracket \mathbf{D} \rrbracket \delta_S = 0, \quad (6)$$

$$(\nabla_{\parallel} \cdot \mathbf{B}_0) \delta_S + \mathbf{n} \cdot \mathbf{B}_0 \partial_n \delta_S + \overline{\nabla \cdot \mathbf{B}} + \mathbf{n} \cdot \llbracket \mathbf{B} \rrbracket \delta_S = 0. \quad (7)$$

Without loss of generality, we can now consider that the interface is surrounded by air (this situation occurs for example in the case of nanohole arrays in slab waveguides [18]) and use the same decomposition of the susceptibilities as the one for the fields in Eq. (3), that is, $\bar{\chi}_{\iota,0}(\mathbf{x}) = \bar{\chi}_{\iota,0}(x, y) \delta_S(\mathbf{x})$ for ι equal to either ee or mm . The $\bar{\chi}_{\iota,0}$ terms are referred to as the surface susceptibility tensors (and are given in meters). Putting this definition into the constitutive relations of Eq. (2), one finds that the first-order fields are linked to the mean value of the regular fields across the interface via the surface susceptibilities (see Sec. III of the Supplemental Material [17], where the full details of the proof are given). Finally, separating the regular and singular terms in Eqs. (4)–(7) we end up with the following C-GSTCs:

$$\mathbf{n} \times \llbracket \mathbf{E} \rrbracket = -j\omega \mu_0 (\bar{\chi}_{mm,0} \{ \mathbf{H} \})_{\parallel} + \nabla_{\parallel} \times (\bar{\chi}_{ee,0} \{ \mathbf{E} \})_{\perp}, \quad (8)$$

$$\mathbf{n} \times \llbracket \mathbf{H} \rrbracket = j\omega \epsilon_0 (\bar{\chi}_{ee,0} \{ \mathbf{E} \})_{\parallel} + \nabla_{\parallel} \times (\bar{\chi}_{mm,0} \{ \mathbf{H} \})_{\perp}, \quad (9)$$

$$\mathbf{n} \cdot \llbracket \mathbf{D} \rrbracket = -\epsilon_0 \nabla_{\parallel} \cdot (\bar{\chi}_{ee,0} \{ \mathbf{E} \})_{\parallel}, \quad (10)$$

$$\mathbf{n} \cdot \llbracket \mathbf{B} \rrbracket = -\mu_0 \nabla_{\parallel} \cdot (\bar{\chi}_{mm,0} \{ \mathbf{H} \})_{\parallel}, \quad (11)$$

where $\{ \cdot \}$ refer to the mean operator with $\{ \mathbf{A} \} = (\mathbf{A}_+ + \mathbf{A}_-)/2$. These boundary conditions suggest that a subwavelength metasurface operates as if effective surface currents [given on the right-hand side of Eqs. (8) and (9)] were present on its surface.

III. SUSCEPTIBILITY SYNTHESIS

GSTCs provide a way to synthesize the optical response of a shaped metasurface to transform any given incident field into user-defined outgoing transmitted and reflected fields (denoted by \mathbf{E}_+^0 and \mathbf{E}_-^0 , respectively). The results of our synthesis are therefore the coefficient values of the C-GSTCs electric and magnetic surface susceptibility tensors $\bar{\chi}_{\iota,0}$ as a function of the position along an arbitrarily shaped surface. Even though this method does not directly provide the geometry of a real metasurface realizing such susceptibilities, it was extensively used throughout the recent years [19–26] to model and investigate metasurface functionalities, including

bianisotropic surfaces and multi-wave-front shaping metasurfaces.

A. Exact method

Solutions for the susceptibilities are obtained by solving the inverse problem in Eqs. (8) and (9). Note that no physical assumption has been made so far to restrict the susceptibility tensor values, leaving us with 12 complex unknown coefficients (due to the symmetry of the susceptibility tensors). Thus, if we consider setting only one incident and one outgoing field, the solution of the inversion problem is undetermined. Equations (8) and (9) only provide four equations in the interface local system of coordinates, indicating that multiple combinations of coefficients could satisfy the equations. To obtain a well-posed inversion problem, the most traditional method consists of relying on physical conditions, including for example symmetries and reciprocity such that the C-GSTCs share the same number of equations and unknown susceptibility coefficients. In the following, we consider tensors such that the tangential curl terms in (8) and (9) vanish. This is a common assumption made with planar GSTC where this term is usually set to zero by taking $\chi_{i,0}^{\alpha z} = \chi_{i,0}^{z\alpha} = 0$ for $\alpha = x, y, z$ when $\mathbf{n} = z$. For nonplanar interfaces a similar assumption is made using the local orthonormal curvilinear basis $(\boldsymbol{\tau}^1, \boldsymbol{\tau}^2, \mathbf{n})$ with tangential vectors $\boldsymbol{\tau}^1$ and $\boldsymbol{\tau}^2$. Given the decomposition of any field \mathbf{A} on S by $\mathbf{A} = (\mathbf{A} \cdot \boldsymbol{\tau}^1)\boldsymbol{\tau}^1 + (\mathbf{A} \cdot \boldsymbol{\tau}^2)\boldsymbol{\tau}^2 + (\mathbf{A} \cdot \mathbf{n})\mathbf{n}$, the assumption of vanishing tangential curl terms in (8) imposes that the matrices $\bar{\chi}_{i,0}$ satisfy

$$(\bar{\chi}_{i,0}\mathbf{A})_{\perp} = [(\bar{\chi}_{i,0}\mathbf{A}) \cdot \mathbf{n}]\mathbf{n} = \mathbf{0}. \quad (12)$$

Introducing now the general decomposition of the susceptibility tensors in any basis \mathcal{B} ,

$$\bar{\chi}_{i,0} = \sum_{\alpha, \beta \in \mathcal{B}} \chi_i^{\alpha\beta} \boldsymbol{\alpha} \otimes \boldsymbol{\beta} \Rightarrow \bar{\chi}_{i,0}\mathbf{A} = \sum_{\alpha, \beta \in \mathcal{B}} \chi_i^{\alpha\beta} (\mathbf{A} \cdot \boldsymbol{\alpha})\boldsymbol{\beta},$$

valid in both Cartesian or curvilinear coordinates considering either $\mathcal{B} = \{x, y, z\}$ or $\mathcal{B} = \{\boldsymbol{\tau}^1, \boldsymbol{\tau}^2, \mathbf{n}\}$, Eq. (12) leads to $\chi_{i,0}^{\alpha n} = 0$ for $\alpha = \boldsymbol{\tau}^1, \boldsymbol{\tau}^2, \mathbf{n}$. With this choice of susceptibility tensor, we drastically simplify the first two C-GSTCs into their compact forms:

$$\mathbf{n} \times \llbracket \mathbf{E} \rrbracket = -j\omega\mu_0 \bar{\chi}_{mm,0} \{\mathbf{H}_{\parallel}\}, \quad (13)$$

$$\mathbf{n} \times \llbracket \mathbf{H} \rrbracket = j\omega\varepsilon_0 \bar{\chi}_{ee,0} \{\mathbf{E}_{\parallel}\}. \quad (14)$$

Setting the off-diagonal terms $\chi_{i,0}^{\boldsymbol{\tau}^1\boldsymbol{\tau}^2}$ and $\chi_{i,0}^{\boldsymbol{\tau}^2\boldsymbol{\tau}^1}$ to zero then leaves only four unknown coefficients in the curvilinear coordinate system. In Cartesian coordinates the susceptibilities are then found for $\boldsymbol{\alpha}, \boldsymbol{\beta} = x, y, z$ as $\chi_{i,0}^{\alpha\beta} = \chi_{i,0}^{\boldsymbol{\tau}^1\boldsymbol{\tau}^1} \boldsymbol{\tau}_\alpha^1 \boldsymbol{\tau}_\beta^1 + \chi_{i,0}^{\boldsymbol{\tau}^2\boldsymbol{\tau}^2} \boldsymbol{\tau}_\alpha^2 \boldsymbol{\tau}_\beta^2$. Given injected and transmitted electromagnetic fields $\mathbf{E}_{\pm}^0, \mathbf{H}_{\pm}^0$, the inversion of C-GSTCs Eqs. (13) and (14) around the interface leads to

$$\begin{aligned} \chi_{ee,0}^{\boldsymbol{\tau}^1\boldsymbol{\tau}^1} &= \frac{-1}{j\omega\varepsilon_0} \frac{\llbracket \mathbf{H}^0 \cdot \boldsymbol{\tau}^1 \rrbracket}{\{\mathbf{E}^0 \cdot \boldsymbol{\tau}^1\}}, & \chi_{ee,0}^{\boldsymbol{\tau}^2\boldsymbol{\tau}^2} &= \frac{1}{j\omega\varepsilon_0} \frac{\llbracket \mathbf{H}^0 \cdot \boldsymbol{\tau}^2 \rrbracket}{\{\mathbf{E}^0 \cdot \boldsymbol{\tau}^2\}}, \\ \chi_{mm,0}^{\boldsymbol{\tau}^1\boldsymbol{\tau}^1} &= \frac{1}{j\omega\mu_0} \frac{\llbracket \mathbf{E}^0 \cdot \boldsymbol{\tau}^1 \rrbracket}{\{\mathbf{H}^0 \cdot \boldsymbol{\tau}^1\}}, & \chi_{mm,0}^{\boldsymbol{\tau}^2\boldsymbol{\tau}^2} &= \frac{-1}{j\omega\mu_0} \frac{\llbracket \mathbf{E}^0 \cdot \boldsymbol{\tau}^2 \rrbracket}{\{\mathbf{H}^0 \cdot \boldsymbol{\tau}^2\}}. \end{aligned} \quad (15)$$

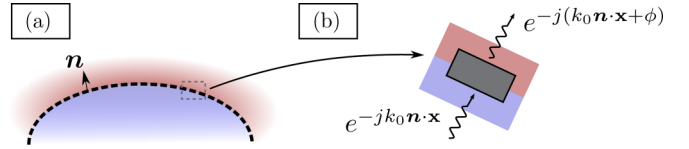


FIG. 2. Schematic representation of a conformal metasurface made of “perfect” meta-atoms with well-controlled phase changes.

B. Phase-based method

One difficulty with the synthesization method of Eq. (15) is that the resulting susceptibilities have a nonzero imaginary part, meaning that suitable loss and gains need to be implemented in the metasurface. We explain in this section how to adapt the phase-based method described in [24] in order to synthesize real-valued susceptibilities. The idea is to consider “perfect” meta-atoms with a transmission equal to 1 and phase shift ϕ as represented in Fig. 2. For a two-dimensional electric field polarized in the (out-of-plane) y direction, we have

$$\begin{aligned} \mathbf{E}_{y,-}^0 &= e^{-jk_0 \mathbf{n} \cdot \mathbf{x}}, \\ \mathbf{H}_{\parallel,-}^0 &= -\frac{1}{\mu_0 c} \mathbf{n} \times \mathbf{y} \mathbf{E}_{y,-}^0, \\ \mathbf{E}_{y,+}^0 &= e^{-j(k_0 \mathbf{n} \cdot \mathbf{x} + \phi)}, \\ \mathbf{H}_{\parallel,+}^0 &= -\frac{1}{\mu_0 c} \mathbf{n} \times \mathbf{y} \mathbf{E}_{y,+}^0. \end{aligned}$$

Once reported in (15), we find that all susceptibilities are equal to [using that $(e^{-j\phi} - 1)/(e^{-j\phi} + 1) = -j \tan(\phi/2)$ and $(\mathbf{n} \times \mathbf{y}) \cdot \boldsymbol{\tau}^1 = -1$ in two dimensions]

$$\chi = -\frac{2}{k_0} \tan\left(\frac{\phi}{2}\right).$$

The susceptibilities are thus found by first computing the expected phase shift ϕ along the (conformal) metasurface. Examples using this method are reported in Secs. VI A 4 and VI B 2 of the Supplemental Material [17].

IV. FINITE-ELEMENT IMPLEMENTATION

To verify the validity of our C-GSTC derivation we implemented these equations using the FEM and tested the performance of the synthesized interfaces in terms of angular response efficiency. Incidentally, and to the best of our knowledge, only a recent work dealing with FEM modeling of planar GSTCs in two dimensions has been proposed [27]. Here, we provide a full three-dimensional modeling method that applies to both planar and conformal interfaces. This modeling method relies on the FEM and thus on the variational formulation associated with the vectorial form of the wave equation. In general, this formulation is given in the frequency domain as

$$\sum_{D \in \mathcal{D}} \int_D \frac{1}{\mu} \nabla \times \mathbf{E} \cdot \nabla \times \boldsymbol{\phi} - k^2 \varepsilon \mathbf{E} \cdot \boldsymbol{\phi} d\mathbf{x} + B_{\partial D} = 0, \quad (16)$$

where \mathcal{D} is the set of domains present in the simulation and $B_{\partial D}$ is a surface integral accounting for the boundary

conditions on the domains borders ∂D and given by

$$B_{\partial D} = -j\omega\mu_0 \int_{\partial D} \mathbf{n} \times \mathbf{H} \cdot \boldsymbol{\phi} ds.$$

At the interface $\partial D_1 \cap \partial D_2$ between two domains, the natural transition conditions give $\mathbf{n} \times \llbracket \mathbf{H} \rrbracket = \mathbf{0}$, thus canceling out the surface integral. With the C-GSTCs however, the jumps of the components of the fields are not equal to zero and $B_S \neq 0$ (with S the C-GSTC interface). From Eqs. (13) and (14) one finds (see Sec. V of the Supplemental Material [17]) that $B_S = B_S^{ee,1} + B_S^{ee,2} + B_S^{mm,1} + B_S^{mm,2}$ with

$$B_S^{ee,\ell} = - \int_S k_0^2 \chi_{ee,0}^{\tau^\ell \tau^\ell} \{ \mathbf{E} \cdot \boldsymbol{\tau}^\ell \} \{ \boldsymbol{\phi}^* \cdot \boldsymbol{\tau}^\ell \} ds,$$

$$B_S^{mm,\ell} = \int_S (\chi_{mm,0}^{\tau^\ell \tau^\ell})^{-1} \llbracket \mathbf{E} \cdot \boldsymbol{\tau}^\ell \rrbracket \llbracket \boldsymbol{\phi}^* \cdot \boldsymbol{\tau}^\ell \rrbracket ds,$$

where $\bar{\ell} = 1$ if $\ell = 2$ and 1 otherwise. One modification of the FEM scheme is also required in order to account for these surface integrals. Indeed, the Nédélec elements usually considered in electromagnetic FEM simulations [28,29] ensure that the natural transition conditions are verified; it considers the same degrees of freedom for the tangential components of the electric field on each side of the interfaces. To account for the C-GSTCs, we instead discretized separately the two domains on each side of S so as to duplicate the number of degrees of freedom for the tangential components and thus make it possible to have a nonzero jump of the fields on S . The surface integrals in B_S together with (16) and additional boundary conditions at the edge of the simulation area to generate an input plane wave and to absorb all outgoing waves (open system) define the whole simulation problem. With respect to existing works dealing with GSTC equations that replace metasurface discontinuous regions with small equivalent volumes (Sec. IV B of Ref. [30]; Sec. IV of Ref. [23]), our approach implements directly the real transition conditions inside the variational formulation. Our FEM simulations were performed using COMSOL Multiphysics in both two and three dimensions [31].

V. NUMERICAL EXAMPLES

The ability to design arbitrary shaped functional interfaces is of particular interest to study the impact of freeform geometry and compare their performance with respect to conventional flat optical components. We have first realized two simple studies of the usual optical components, a lens and a deflector, to illustrate the impact of interface geometry and how it influences the device optical performance.

A. Deflector

In this first example, we consider a periodically oscillating interface designed using C-GSTCs from which an incident plane wave is refracted at an angle of $\theta_r \simeq 45^\circ$ (the precise value of θ_r is given by the order of diffraction) with respect to the z axis. We synthesized the susceptibilities using (15) considering z -polarized input and output plane waves and the output one given by an order of diffraction with angle θ_r . The interface geometry is given by $f(x, y) = \alpha \cos(\frac{2\pi}{5\lambda}x)$ for α ranging from 0 to 2.5λ . We implemented the C-GSTC FEM

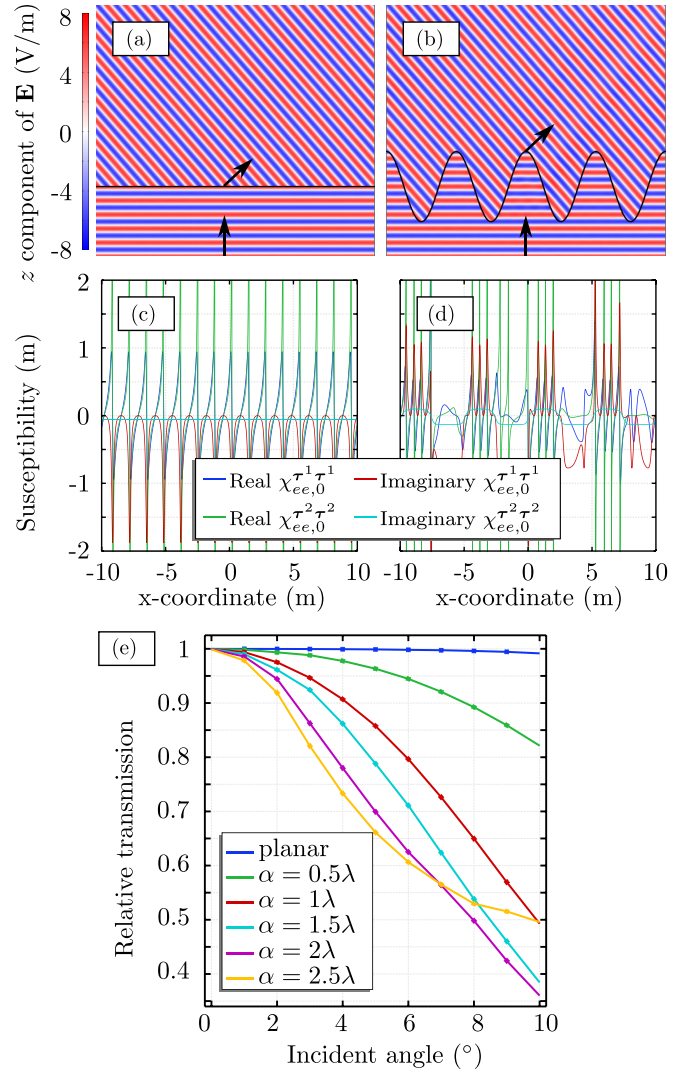


FIG. 3. Planar and sinusoidal light deflectors. (a) Flat metasurface deflecting light at an angle θ_r° . (b) Similar calculation to that in (a) but considering a sinusoidal (conformal) interface. (c) and (d) Associated electric susceptibilities (here $\bar{\chi}_{ee} = \bar{\chi}_{mm}$) for both planar and conformal metasurfaces. (e) Sensitivity of the transmission (normalized by the total output power) into the θ_r° order of diffraction depending on the amplitude α of the interface's sinusoidal oscillations.

as mentioned above considering a simulation domain size of $20\lambda \times 20\lambda$ and the results are summarized in Fig. 3.

As we can see in Fig. 3(e) the sinusoidal interface does not perform well when the plane wave is sent with an incident angle different than zero. More precisely, we can see that its performance drastically reduces the deflection efficiency from 100% to only 50% for less than 10° incident angle change.

B. Lens

This example is inspired from pioneering work realized by Abbe back in 1881 [32]. It states that for any optical system, which would be able to produce on- and off-axis sharp images, the ratio of the sines of the entrance and exit angles ($\alpha_{in}, \alpha_{out}$) of optical rays must equal the magnification M of the

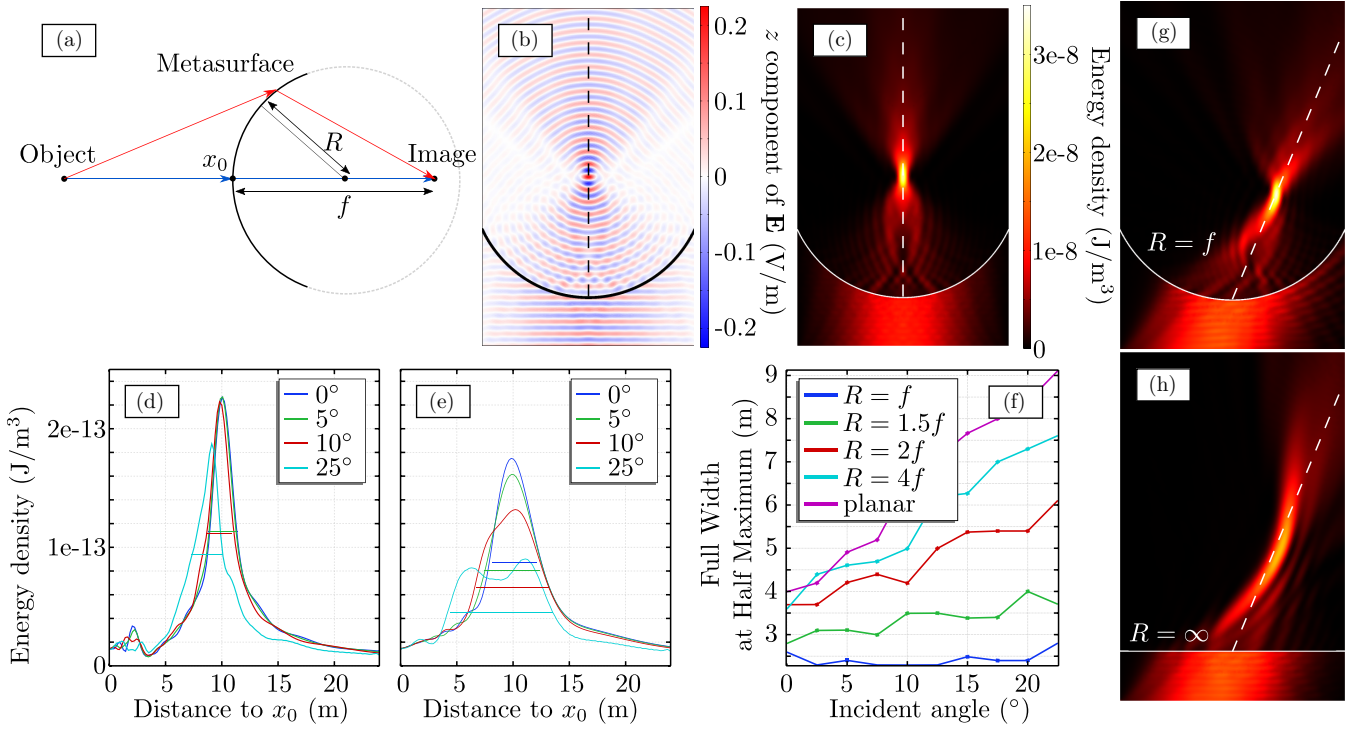


FIG. 4. Planar and conformal metalenses. (a) Schematic of the Abbe-sine numerical experiment realized with curved metalens. (b) and (c) Calculation of the field transmitted through a synthesized conformal metalens when $R = f$. (d) Focusing profile [dashed lines in (b)–(c) and (g)–(h), respectively] of the curved metalens when $R = f$. (e) Same as (d) for the planar metalens. (f) Sensitivity of the full width at half maximum with respect to the incident angle for different radii of curvature of the metasurface. (g) and (h) Same calculation as in (c) but using a plane wave tilted by 22.5° while adjusting the surface curvature to $R = f$ and $R = \infty$, respectively.

optical system with the relationship $\sin(\alpha_{\text{in}})/\sin(\alpha_{\text{out}}) = |M|$. Ray-tracing calculations of light focusing from curved metasurfaces have suggested that the Abbe-sine condition can be realized for spherical interface with radius of curvature equal to the focusing distance of the curved metalens [33,34]. The C-GSTCs proposed herein have been utilized to calculate the susceptibilities of a focusing half-circle metalens and are used to study the angular response of the Abbe-sine component. We thus consider the focusing of an incident plane wave from a metalens covering a hemisphere centered at $(0, 0, R)$ with radius R while imposing a spherical output wave centered at the focal point $(0, 0, f)$. The simulation results are provided in Figs. 4(b) and 4(c) using a domain size of $10\lambda \times 30\lambda$ with $f = 10\lambda$.

To reach the Abbe-sine condition with curved interfaces, it is necessary to study the focusing responses of the metalens for arbitrary incident angles, while keeping the surface susceptibilities initially calculated for a normally incident beam. The comparison of both planar versus curved focusing efficiency is presented in Figs. 4(d) and 4(e), including a quantitative comparison with the evolution of the full width at half maximum (FWHM) in Fig. 4(f). It indicates that the FWHM of the conformal metasurface is almost invariant with respect to the incident angle while it increases for the planar interface case as a function of the incident angle from 0 to 20° . Conformal metasurfaces are thus able to improve the focusing profile and the point-spread function to reduce monochromatic aberrations. In Sec. VI of the Supplemental Material [17] we also present incident angle characterization

of sinusoidal interfaces that are traditionally used for light deflection in generalized Snell-law experiments. We show that instead, their deflection efficiency is extremely sensitive to the incident angles.

C. Cloaking

In our third example, we realize a new sort of optical illusion, manipulating the optical signature of an actual object, for example a cat-shaped structure, to mimic light scattering of another object, a mouse-shaped structure. Applying a metasurface conformally to the shape on the former object, one can realize an advanced version of cloaking accounting for both the complex shapes and projection of arbitrary field distributions. Our approach suggests wrapping a metasurface conformally to an object, while adjusting the surface susceptibilities, to reflect and/or transmit light as if it was coming from another user-defined object.

The synthesizing of the susceptibilities is realized by computing first the electromagnetic fields scattered by both objects, i.e., cat and mouse shaped nanostructures in the absence of a metasurface [see Figs. 5(c) and 5(d)], considering an incident plane wave impinging from the bottom left of the simulation domain. We then apply the inversion procedure to adjust the interior fields from the cat geometry to the exterior fields scattered by the mouse-shaped structure through the conformal susceptibilities disposed along the cat surface [see Fig. 5(e)]. The calculations are performed considering a background domain with permittivity equal to $\epsilon_r = 1$ and

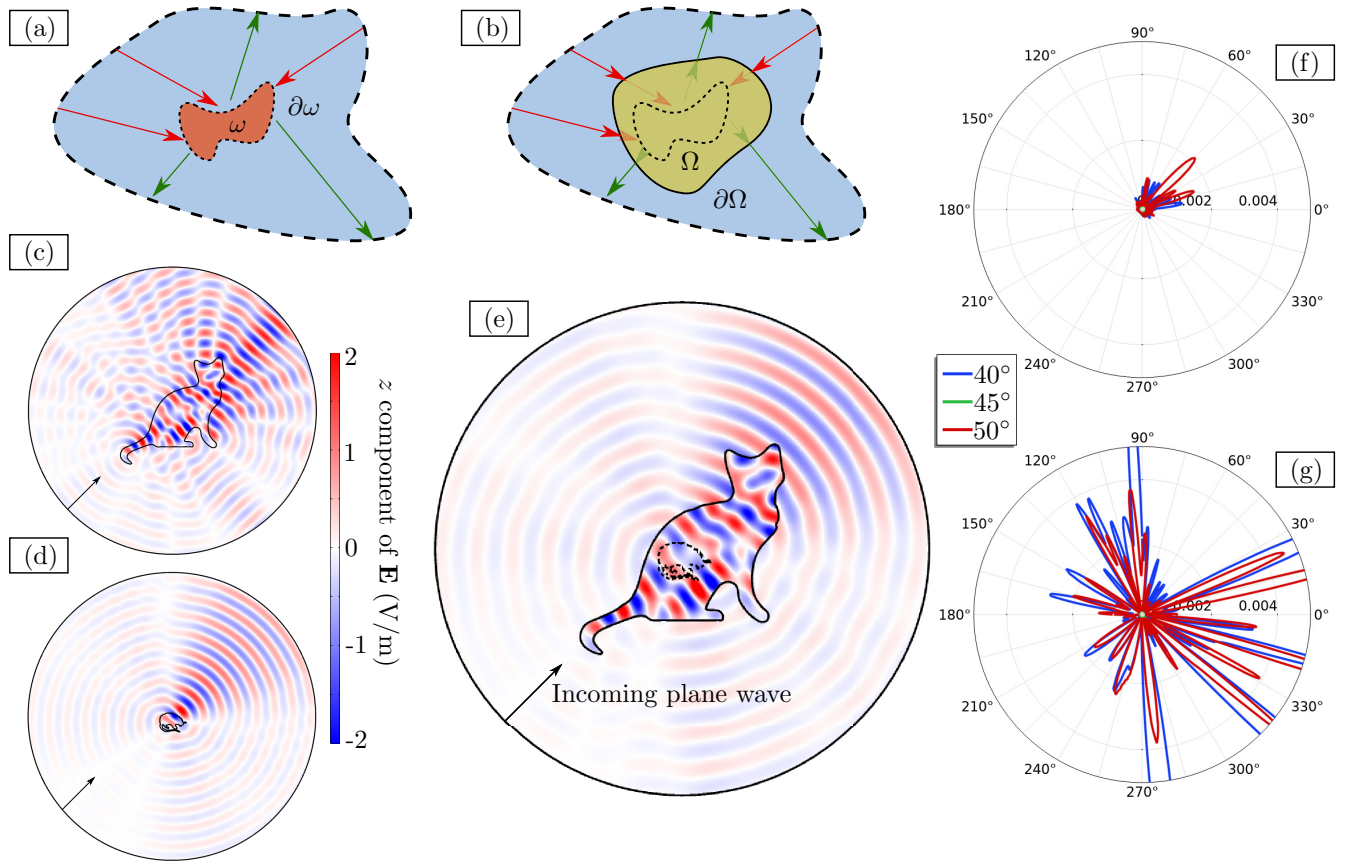


FIG. 5. Conformal metasurface making the cat reflections look like the ones coming from a virtual mouse. (a) and (b) Schematic representation of the system: a shape Ω with an optical index equal to 2 is coated with a conformal metasurface on its borders $\partial\Omega$ with susceptibilities synthesized in such a way that the reflections produced by this shape are equal to the one from a nonmodified shape ω with the same optical index. (c) and (d) Simulation of the reflected field for Ω (resp. ω) representing a cat (resp. a mouse). (e) Simulation of the C-GSTC coated Ω shape (ω given for comparison with dashed lines). (g) Absolute difference of the outgoing Poynting vector's normal component on the exterior circle between the field reflected by the ω shape and the C-GSTC coated Ω one. (f) Same as (g) but imposing a zero electric field inside the Ω shape during the susceptibility synthesization step.

assuming that the objects are made of homogeneous medium with a permittivity $\epsilon_r = 2$. The results summarized in Fig. 5 thus indicate that the mouse-scattered fields are reproduced almost perfectly, even from an arbitrary shaped structure, producing the illusion of light scattering from a different object. For practical applications, it is necessary to verify that the scattering illusion is preserved over a relatively large incident angle range. Figure 5(g) presents the angular cross sections as a function of the incident angles (the outward Poynting vector norm) computed on the edge of the simulation domain (circle boundary). Figure 5(g) shows that the performance of the illusion system behaves poorly for incident angles slightly different from the designed case. Note that here the susceptibilities have been calculated considering that the field inside the cat-shaped nanostructure remains equal to the field distribution in the absence of a beam-shaping metasurface. Choosing another inner field distribution is also possible. As an example, to study designs with reduced angular sensitivity, we show in Fig. 5(f) that imposing a zero field inside the shaped nanostructure could maintain broader angular scattering [41–43].

VI. CONCLUSION

In conclusion, we have proposed a detailed derivation and full wave implementation of conformal GSTCs. We proposed several numerical examples showing the versatility of the inversion procedure with C-GSTCs. Our proposed modeling technique may be of interest to scientists and engineers searching for innovative solutions to adjust the optical response of freeform optical components. However, it is important to keep in mind that even if the presented numerical results may seem promising for future applications of conformal metasurfaces, the susceptibilities obtained through the inversion procedure are not directly linked to physical materials or structures. Furthermore, our numerical examples have shown that spatially varying complex susceptibilities need to be considered, suggesting that a dedicated number of gains and losses have to be carefully distributed along the surface to match incoming with outgoing fields. In Sec. III B, we have proposed a synthesization method based on phase shifts which lead to real-valued susceptibilities. Numerical experiments (whose results are given in the Supplemental Material [17]) show that this method still allows one to control the

transmitted fields at the expense of small losses. Other synthesis methods which rely on more practical parameters could also be considered and adapted to conformal geometries. As such, we can cite methods based on reflection and transmission coefficients such as in [24,35–37] or the method in [38] which relies on a Lorentzian model of the susceptibilities. Lastly, susceptibilities of real metasurfaces could also be

obtained through the use of the homogenization theory such as in Refs. [39,40].

ACKNOWLEDGMENT

The authors acknowledge support from the French defense procurement agency under the ANR ASTRID Maturation program, Grant Agreement No. ANR-18-ASMA-0006-01.

-
- [1] W. Cai, U. K. Chettiar, A. V. Kildishev, and V. M. Shalaev, *Nat. Photon.* **1**, 224 (2007).
- [2] D. R. Smith, J. B. Pendry, and M. C. Wiltshire, *Science* **305**, 788 (2004).
- [3] M. Scalora, G. D'Aguanno, N. Mattiucci, M. J. Bloemer, D. de Ceglia, M. Centini, A. Mandatori, C. Sibilia, N. Akozbek, M. G. Cappeddu *et al.*, *Opt. Express* **15**, 508 (2007).
- [4] N. Yu, P. Genevet, M. A. Kats, F. Aieta, J.-P. Tetienne, F. Capasso, and Z. Gaburro, *Science* **334**, 333 (2011).
- [5] J. B. Pendry, D. Schurig, and D. R. Smith, *Science* **312**, 1780 (2006).
- [6] P. Genevet, F. Capasso, F. Aieta, M. Khorasaninejad, and R. Devlin, *Optica* **4**, 139 (2017).
- [7] Q. Song, S. Khadir, S. Vézian, B. Damilano, P. Mierry, S. Chenot, V. Brandli, and P. Genevet, *Sci. Adv.* **7**, eabe1112 (2021).
- [8] Q. Song, A. Baroni, R. Sawant, P. Ni, V. Brandli, S. Chenot, S. Vézian, B. Damilano, P. de Mierry, S. Khadir *et al.*, *Nat. Commun.* **11**, 1 (2020).
- [9] V. A. Markel, *J. Opt. Soc. Am. A* **33**, 1244 (2016).
- [10] J. C. Maxwell Garnett, *Philos. Trans. R. Soc. London A* **203**, 385 (1904).
- [11] P. A. Tirkas and K. R. Demarest, *IEEE Trans. Antennas Propag.* **39**, 1338 (1991).
- [12] J. G. Maloney and G. S. Smith, *IEEE Trans. Antennas Propag.* **41**, 690 (1993).
- [13] M. Duruflé, V. Péron, and C. Poignard, *Commun. Comput. Phys.* **16**, 213 (2014).
- [14] M. Idemen, *J. Phys. Soc. Jpn.* **59**, 71 (1990).
- [15] M. Dehmollaian and C. Caloz, in *Proceedings of the 2019 IEEE International Symposium on Antennas and Propagation and USNC-URSI Radio Science Meeting* (IEEE, 2019), pp. 1323–1324.
- [16] Y. Zhang and Y. Tong, *Opt. Commun.* **483**, 126590 (2021).
- [17] See Supplemental Material at <http://link.aps.org/supplemental/10.1103/PhysRevB.106.035110> for more details regarding the C-GSTC derivation as well as additional information on the numerical tests and implementation.
- [18] J. R. Ong, H. S. Chu, V. H. Chen, A. Y. Zhu, and P. Genevet, *Opt. Lett.* **42**, 2639 (2017).
- [19] K. Achouri, M. A. Salem, and C. Caloz, *IEEE Trans. Antennas Propag.* **63**, 2977 (2015).
- [20] T. J. Smy, S. A. Stewart, and S. Gupta, *IEEE Access* **8**, 93408 (2020).
- [21] G. Lavigne, K. Achouri, V. S. Asadchy, S. A. Tretyakov, and C. Caloz, *IEEE Trans. Antennas Propag.* **66**, 1321 (2018).
- [22] A. Momeni, H. Rajabalipanah, A. Abdolali, and K. Achouri, *Phys. Rev. Appl.* **11**, 064042 (2019).
- [23] X. Jia, Y. Vahabzadeh, C. Caloz, and F. Yang, *IEEE Trans. Antennas Propag.* **67**, 2542 (2019).
- [24] K. Achouri, G. Lavigne, and C. Caloz, *J. Appl. Phys.* **120**, 235305 (2016).
- [25] T. Brown, C. Narendra, Y. Vahabzadeh, C. Caloz, and P. Mojabi, *IEEE Trans. Antennas Propag.* **68**, 1812 (2019).
- [26] K. Achouri and C. Caloz, *Nanophotonics* **7**, 1095 (2018).
- [27] S. Sandeep, J.-M. Jin, and C. Caloz, *IEEE Trans. Antennas Propag.* **65**, 2413 (2017).
- [28] J.-M. Jin, *The Finite-Element Method in Electromagnetics* (John Wiley & Sons, 2015).
- [29] P. Monk, *Finite-Element Methods for Maxwell's Equations* (Oxford University Press, 2003).
- [30] Y. Vahabzadeh, K. Achouri, and C. Caloz, *IEEE Trans. Antennas Propag.* **64**, 4753 (2016).
- [31] The COMSOL models are freely available at the following address: <http://www.sop.inria.fr/atlas/tmp/ComsolPRB.zip>. These models allow for an easy simulation of any planar or conformal GSTCs with given susceptibilities (which can be found through the inversion procedure).
- [32] C. Hockin, *J. R. Microsc. Soc.* **4**, 337 (1884).
- [33] F. Aieta, P. Genevet, M. Kats, and F. Capasso, *Opt. Express* **21**, 31530 (2013).
- [34] C. E. Gutiérrez, L. Pallucchini, and E. Stachura, *J. Opt. Soc. Am. A* **34**, 1160 (2017).
- [35] X. Liu, F. Yang, M. Li, and S. Xu, in *Proceedings of the 2017 IEEE International Symposium on Antennas and Propagation & USNC/URSI National Radio Science Meeting* (IEEE, 2017), pp. 1725–1726.
- [36] S.-G. Lee and J.-H. Lee, *J. Korean Inst. Electromagn. Eng. Sci.* **29**, 685 (2018).
- [37] S. Stewart, Y. L. de Jong, T. J. Smy, and S. Gupta, *IEEE Trans. Antennas Propag.* **70**, 1265 (2022).
- [38] V. Tiukuvaara, T. J. Smy, and S. Gupta, in *Proceedings of the 2020 14th European Conference on Antennas and Propagation (EuCAP)* (IEEE, 2020), pp. 1–4.
- [39] C. L. Holloway, E. F. Kuester, and A. Dienstfrey, *Radio Sci.* **49**, 813 (2014).
- [40] N. Lebbe, K. Pham, and A. Maurel, *IEEE Trans. Antennas Propag.*, 1 (2022).
- [41] A. Henrot and M. Pierre, *Variation et Optimisation de Formes: Une Analyse Géométrique* (Springer Science & Business Media, 2006).
- [42] L. Onural, *J. Math. Anal. Appl.* **322**, 18 (2006).
- [43] M. Idemen, *Discontinuities in the Electromagnetic Field* (John Wiley & Sons, 2011).